Three-dimensional Reconstruction of Painted Human Interphase Chromosomes: Active and Inactive X Chromosome Territories Have Similar Volumes but Differ in Shape and Surface Structure

Roland Eils,* Steffen Dietzel,‡ Etienne Bertin,§ Evelin Schröck,‡ Michael R. Speicher,‡ Thomas Ried,‡ Michel Robert-Nicoud,§ Christoph Cremer,*‖ and Thomas Cremer*‡

*Interdisciplinary Center of Scientific Computing (IWR) and Graduierten-Kolleg "Modeling and Scientific Computing in Mathematics and Science," University of Heidelberg, 69120 Heidelberg, Germany; ‡Institute of Human Genetics, University of Heidelberg, 69120 Heidelberg, Germany; §Laboratory DyOGen, UPR-ES EA 2021, Institut Nationale de la Santé et de la Recherche Médicale U309, Institute Albert Bonniot, Université Joseph Fourier, Grenoble 1, France; and ‖Institute of Applied Physics, University of Heidelberg, 69120 Heidelberg, Germany

Abstract. This study provides a three-dimensional (3D) analysis of differences between the 3D morphology of active and inactive human X interphase chromosomes (Xa and Xi territories). Chromosome territories were painted in formaldehyde-fixed, three-dimensionally intact human diploid female amniotic fluid cell nuclei (46, XX) with X-specific whole chromosome composite probes. The colocalization of a 4,6-diamidino-2-phenylindole dihydrochloride–stained Barr body with one of the two painted X territories allowed the unequivocal discrimination of the inactive X from its active counterpart. Light optical serial sections were obtained with a confocal laser scanning microscope. 3D-reconstructed Xa territories revealed a flatter shape and exhibited a larger and more irregular surface when compared to the apparently smoother surface and rounder shape of Xi territories. The relationship between territory surface and volume was quantified by the determination of a dimensionless roundness factor (*RF*). *RF* and surface area measurements showed a highly significant difference between Xa and Xi territories ($P < 0.001$) in contrast to volume differences ($P > 0.1$). For comparison with an autosome of similar DNA content, chromosome 7 territories were additionally painted. The 3D morphology of the two chromosome 7 territories was similar to the Xa territory but differed strongly from the Xi territory with respect to *RF* and surface area ($P < 0.001$).

While small scale chromatin structures from the level of nucleosomes to the level of the 30-nm fiber have been explored in detail, knowledge about the large scale organization of chromatin is still scarce or hypothetical (Manuelidis, 1990; Saitoh and Laemmli, 1994). Advances in molecular cytogenetics have provided the means to fill this gap. Chromosome "painting" with whole chromosome composite DNA probes has demonstrated that each interphase chromosome occupies a distinct territory in the human cell nucleus (Cremer et al., 1988; Lichter et al., 1988; Pinkel et al., 1988, Jauch et al., 1990). In situ hybridization with chromosome-specific subregional DNA probes has indicated a dynamic intranuclear organization and nonrandom distribution of chromosomal subdomains, such as centromeric heterochromatin, during the cell cycle and in postmitotic cells (Manuelidis, 1984; Manuelidis and Borden, 1988; Ferguson and Ward, 1992; Hulspas et al., 1994; Dietzel et al., 1995). Recently, topological relationships between chromosome territories or genes and other defined nuclear domains, such as splicing domains (Spector, 1993), have become a focus of interest (Cremer et al., 1993; Xing et al., 1993; Zirbel et al., 1993; Kurz et al., 1996). In spite of this progress, knowledge of the large scale organization of chromatin in the cell nucleus is presently not sufficient to permit an unequivocal connection with nuclear functions.

The two X territories in female somatic cell nuclei provide a case for experimental attempts to study the three-

Address all correspondence to Thomas Cremer, Institut für Anthropologie und Humangenetik, Ludwig Maximilians Universität, Richard Wagner Str. 10/I, D-80333 München, Germany. Tel.: 49-89-5203381. Fax: 49-89-4203389.

Steffen Dietzel's present address is Center of Molecular Biology, University of Heidelberg, INF 282, 69120 Heidelberg, Germany.

Evelin Schröck and Thomas Ried's present address is Diagnostic Development Branch, National Center for Human Genome Research, 49 Convent Drive, Bethesda, MD 20892-4470.

dimensional (3D)[1] structure of two homologous chromosome territories with distinctly different transcriptional acivities. In mammals, one X chromosome (Xi) becomes genetically inactivated during early development, while the other (Xa) remains genetically active (Lyon, 1961; Gartler and Riggs, 1983; Rastan, 1994). Only a small fraction of genes on Xi escapes inactivation including the genes located in the pseudoautosomal region at Xp22.3 and a few other sites (for reviews see Rappold, 1993; Disteche, 1995). Xi (or part of it) can be identified as an intensely stained structure of facultative heterochromatin called the Barr body (Barr and Bertram, 1949; Brown, 1966). At face value, the distinctly different behavior of active and inactive X chromosomes noted in Barr body staining procedures argues for a global difference in chromatin condensation (for review see Gartler and Riggs, 1983). It has been assumed that facultative and constitutive heterochromatin is much more condensed than euchromatin in interphase nuclei, but the suggested difference (5–10×) has not been well documented. If such a figure were to be applied to entire Xa and Xi territories, one would expect a corresponding difference in the fraction of the nuclear volume occupied by the two chromosomes. A few authors have suggested that heterochromatin owes its bulk to accessory material rather than to differential DNA condensation (Muller and Gershenson, 1935; for reviews see Cooper, 1959; Brown, 1966).

Recently, we and others (Ikizyan et al., 1994) have combined light optical serial sectioning of painted human chromosome territories and 3D image analysis procedures to estimate territory volumes in various human cell types. In contrast to our expectation, we obtained similar volumes for both X territories in female cell nuclei (Bischoff et al., 1993; Eils et al., 1995*a*; Rinke et al., 1995). Here, we describe the results of a more detailed study of 3D-morphology differences between Xi and Xa territories in three-dimensionally preserved female human amniotic fluid cell nuclei. Xi territories were identified by their colocalization with a 4,6-diamidino-2-phenylindole dihydrochloride (DAPI)–stained Barr body. For comparison we investigated the 3D morphology of chromosome 7 territories. This autosome was chosen because its relative DNA content per diploid genome is similar to the X chromosome (2.7% for a single chromosome 7 vs. 2.5% for a single X; Morton, 1991). Our findings demonstrate a 3D morphology difference between the two X territories. 3D-reconstructed Xa territories had a flatter shape and a larger, apparently more complexly folded surface than Xi territories. Chromosome 7 territories appeared more similar to the Xa territory than to its inactive counterpart.

Materials and Methods

Cell Material

Primary human amniotic fluid cell cultures with a normal female karyotype (46,XX) were subcultured on glass slides. Growing subcultures were fixed with buffered formalin (4% formaldehyde solution in 1× PBS for 5 min). Several permeabilization steps were performed to achieve strong painting of entire chromosome territories with little background. Formalin-fixed cells were treated twice with Triton X-100/Saponin (0.1% each, 5 min), washed in 0.1 M Tris-HCl (pH 7.2), equilibrated in 20% glycerol in 1× PBS for 20 min, freeze–thawed by briefly dipping three times in liquid nitrogen, and stored at 4°C in 1× PBS containing 0.04% sodium azide. Before chromosomal in situ suppression (CISS) hybridization, cells were pretreated with pepsin (50 mg/ml) in 0.01 M HCl, pH 2.0, at 37°C and postfixed with 1% PBS-buffered formalin (for 10 min). In some experiments, 1 M NaSCN was applied overnight before pepsin digestion without notable effects on the 3D morphology. Control experiments showed that the extent of DNA cross-linking induced by fixation with 4% buffered formalin was sufficient to maintain the size and shape of amniotic fluid cell nuclei as well as the positioning of intranuclear structures, such as nucleoli and centromeres under these conditions (Cremer et al., 1993; Scherthan and Cremer, 1994).

DNA Probes and Labeling

Whole chromosome composite DNA probes for human chromosomes 7 and X were prepared from chromosome-specific plasmid libraries kindly provided by Dr. J. Gray (University of California, San Francisco, CA; Collins et al., 1991). The alphoid DNA probe p7t1 delineates the centromeric region of chromosome 7 (Waye et al., 1987) and was a gift from Dr. H.F. Willard (Case Western Reserve University, Cleveland, OH). Probes were labeled using standard nick translation assays (Lichter and Cremer, 1992) with Biotin-16-dUTP (Boehringer Mannheim Corp., Indianapolis, IN) or Digoxigenin-11-dUTP (Boehringer Mannheim Corp.)

CISS Hybridization and Probe Detection

CISS hybridization was carried out as previously described (Lichter and Cremer, 1992) using unlabeled Cot-1 DNA (1.5 μg/μl) and a high amount of labeled DNA probes to maximize the hybridization efficiency (60–200 ng DNA/μl of pBS libraries and 1 ng DNA/μl of the p7t1 alphoid DNA probe). 10 μl hybridization mixture was applied overnight to a 18 × 18 mm slide area. Biotinylated DNA sequences were visualized with Avidin-FITC or Avidin-TRITC (both from Vector Labs, Inc., Burlingame, CA). Digoxigenin-labeled sequences were detected with mouse-anti-Digoxigenin antibodies (Sigma Chemical Co., St. Louis, MO) and TRITC- or Cy5-conjugated goat anti–mouse IgG (Boehringer Mannheim Corp. or Jackson ImmunoResearch Laboratories Inc., West Grove, PA). Barr body staining was performed with DAPI (Dyer et al., 1989). The slides were mounted in fluorescence–antifading solution (PBS/glycerol [1/9,vol/vol] containing 0.1% 1,4-phenylendiamine-dihydrochloride; Serva Biomedicals, Paramus, NJ). Only experiments where the large majority of nuclei revealed a strong painting of chromosome territories and little background were deemed acceptable for further evaluation. To maintain the 3D nuclear topography, air drying was carefully avoided during the fixation, permeabilization, in situ hybridization, and detection procedures.

Image Recording of Barr Bodies and Chromosome Territories

The localization of the Barr body was either documented before CISS hybridization with a cooled charge coupled device (CCD) camera (Photometrics, Tucson, AZ) coupled to an epifluorescence microscope (Axiophot; Carl Zeiss, Inc., Thornwood, NY) (experiment 1, 3a) or by drawings of the DAPI-stained nuclei after CISS hybridization (experiment 2). In all cases, the recognition of a true Barr body was confirmed by its colocalization with a painted X territory. Nuclei where the expected colocalization could not be confirmed were rare and excluded from further consideration. Series of light optical sections were recorded for each nucleus with a three channel confocal laser scanning microscope (TCS; Leica, Inc., Deerfield, IL) equipped with a Plan Apo 63×/1.4 oil immersion lens. Using the appropriate lines of an argon/krypton laser (488, 567, and 647 nm) for the visualization of FITC, TRITC, and Cy5, respectively, stacks of 512 × 512 or 256 × 256 equidistant 8-bit grayscale images were obtained. To improve the signal-to-noise ratio, each line was scanned 16 times and averaged. In experiment 1, light optical serial sectioning of the X chromosome territories was carried out at an axial distance of 300 nm. In experiments 2 and 3, optical sections were obtained at an axial distance of 250 nm. Depending on the height of the respective nucleus, each stack consisted of 12 to 30 images. Image stacks were stored on a magneto-optical disk and transferred to a workstation (SGI IRIS INDIGO, CPU R4000, 100 MHz, 64 MB RAM, Elan-Graphics; Silicon Graphics, Inc., Moutain View, CA).

1. *Abbreviations used in this paper*: 3D, three-dimensional; CISS, chromosomal in situ suppression; DAPI, 4,6-diamidino-2-phenylindole dihydrochloride; *RF*, roundness factor; *S*, surface; *V*, volume.

3D Image Analysis of Painted Chromosome Territories

For a quantitative analysis of painted chromosome territories, a Voronoi tessellation approach was applied (Eils et al., 1995*a*; for a general description of Voronoi diagrams and their applications see Okabe et al., 1992). Fig. 1, *a–f*, exemplifies the application of this approach to a single light optical nuclear section with two painted X territories (see Eils et al., 1995*a* and legend to Fig. 1). The neighborhood relationship of polygons in the resulting Voronoi diagram (Fig. 1 *g*, *solid lines*) is described by the Delaunay graph, which is built in parallel with the Voronoi diagram. In the Delaunay graph, all generators from neighboring polygons, i.e., polygons sharing a common edge, are connected (Fig. 1 *g*, *dashed lines*). The Delaunay graph represents the complete neighborhood information of the Voronoi diagram and is used for the rapid extraction of image objects that consist of clusters of polygons with mean gray value intensities above a certain threshold.

In this study, a 3D Voronoi tessellation procedure was carried out. For this purpose the 3D image volume represented by the stack of light optical serial sections from a given cell nucleus was iteratively tessellated into polyhedra. Each polyhedron represents a subvolume with voxels of similar gray value intensities. Chromosome territories were extracted by a search for connected polyhedra in the corresponding Delaunay graph. Two neighboring polyhedra were regarded to belong to the same object, if the associated mean gray value of all voxels belonging to each polyhedron exceeded a common preset gray value threshold. After 3D segmentation, chromosome territory volume (V), surface (S), and a roundness factor (RF) were computed. RF is defined as

$$RF = 36\pi\frac{V^2}{S^3},\ 0 < RF \leq 1.$$

Tessellation of the image stacks into polyhedra largely reduces the amount of data to be handled by the computer to visualize 3D objects such as chromosome territories by ray tracing (Quien and Müller, 1992) and is particularly suited to calculate volume, surface, and shape parameters.

Results

To compare the size and 3D morphology of painted active and inactive X chromosome territories, 67 female amniotic fluid cell nuclei with two well separated X territories and a clearly recognizable Barr body were selected by investigator S. Dietzel and subjected to laser confocal serial sectioning (12 nuclei in experiment 1, 42 in experiment 2, and 13 in experiment 3a). Fig. 2 *a* shows laser confocal serial sections through a typical nucleus with painted X chromosome territories together with a microphotograph of the DAPI-stained Barr body. A second investigator (R. Eils) carried out the quantitative image analysis procedure without knowledge of the Barr-body assignment to one of the two X territories. In experiment 2, image analysis data obtained for 84 X territories were compared with the data for simultaneously painted chromosome 7 territories. In experiment 3b, light optical serial sectioning was performed for an additional random sample of 56 nuclei for which a Barr body was not recorded.

Comparison of Chromatin Condensation Patterns Between Xa, Xi, and Chromosome 7 Territories

Light optical sections through painted chromosome territories were inspected at different threshold levels. Fig. 3, *a–l*, presents typical examples for optical sections through X territories. At very low thresholds (*a*, *e*, and *i*), the territories started to merge with the surrounding background. Segmentation of territory borders could be easily performed for a range of intermediate threshold levels (*b*, *c*, *f*, *g*, *j*, and *k*; see also below). In some nuclei, Xi territory sections showed a densely painted territory core surrounded by a rim of less densely painted DNA, while Xa territory sections revealed intensely painted subregions interspersed with weakly painted ones. When compared to the borders of Xi territories, Xa territory borders appeared considerably more irregularly shaped with both convex and concave segments and apparent infoldings. At very high thresholds, only the core of the Xi territory was visible and the Xa territory no longer appeared as a coherent structure, but showed numerous separate and intensely painted dots (*d*, *h*, and *l*). Sections through chromosome 7 territories showed a chromatin condensation pattern and surface configuration similar to Xa territories (for an example see Fig. 3, *m–p*). These data suggest similarities in chromatin condensation patterns between Xa and chromosome 7 territories but strong differences between Xa and Xi territories.

3D-reconstructed Xa and Xi Territories in Barr Body–Positive Cell Nuclei Reveal Similar Volumes but Differences in Shape and Surface

For each painted chromosome territory present in 123 light optically sectioned nuclei, we computed its territory volume (V), its surface area (S), and roundness factor (RF). RF ($1 \geq RF > 0$) is a dimensionless factor and provides a measure for the relative size of the chromosome territory volume normalized by its surface (see Materials and Methods). $RF = 1$ describes the relationship for an ideal sphere and $RF = 0$ for an infinitely extended structure. Two chromosome territories with the same volume but different RF values differ in at least one of two features, which affect the volume to surface relationship: A territory with the smaller RF value may have a flatter shape and/or a more irregular surface structure with protrusions and infoldings.

A description of the 3D morphology of X chromosome territories in quantitative rather than qualitative terms has been a major goal of our studies. The nucleus presented in Fig. 2 may serve as a case in point that intuitive judgments of chromosome territory volumes can be strongly misleading. Individual light optical sections consistently show a smaller diameter for the Xi territory than for its active counterpart, suggesting a smaller Xi territory volume. A closer inspection of the entire stack of sections however, reveals that the Xi territory is present in all light optical nuclear sections from top to bottom, while the apparently more extended Xa territory is considerably flatter and only seen in a few sections. 3D reconstructions of both X territories from this nucleus performed at a median threshold level (Fig. 2, *b–e*) yielded a slightly larger volume for Xi (Fig. 6 *a*, experiment 1, nucleus No. 9), while Xa showed a larger surface area and RF value (Fig. 6, *b* and *c*).

For each nucleus, the upper and lower limit of the threshold range useful for the segmentation of chromosome territories was interactively defined (compare Fig. 3): The upper limit was set to the threshold value where components of a chromosome territory connected at a lower threshold started to fall apart. Volumes recorded at higher thresholds would underestimate the true volume, since only chromosomal subregions with high painting intensi-

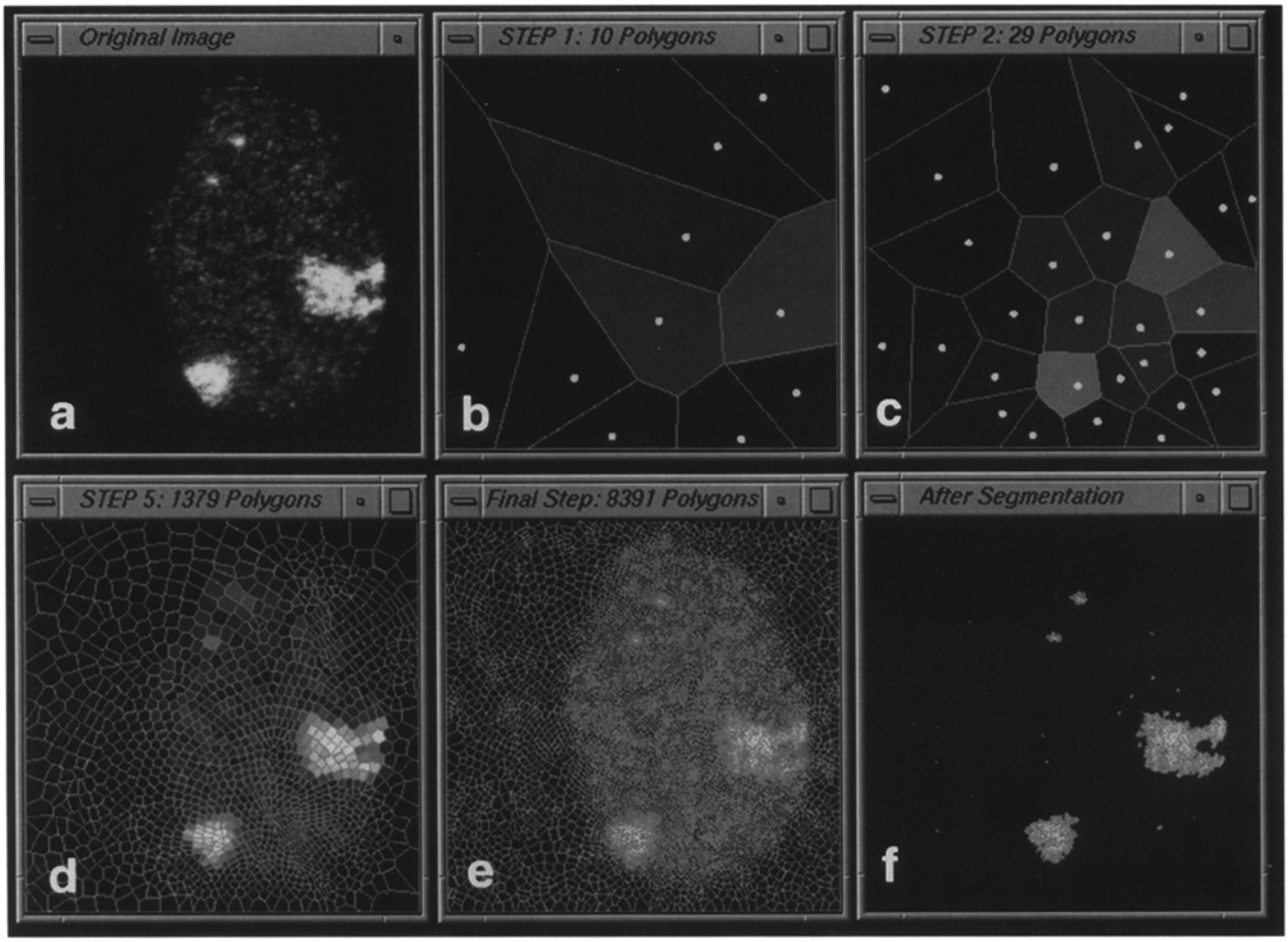

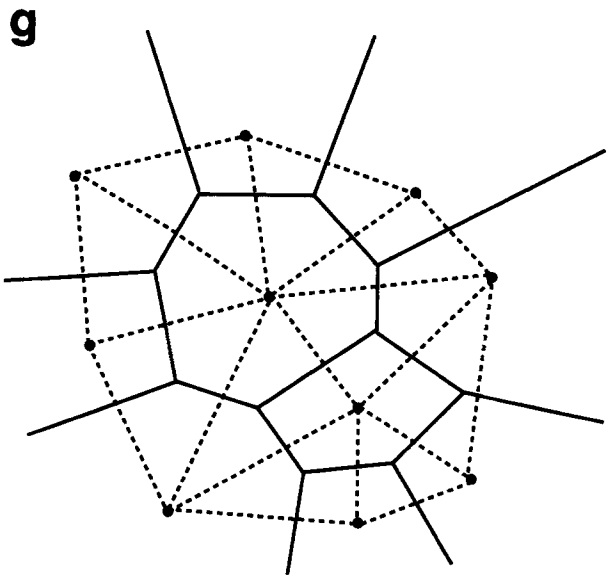

Figure 1. Iterative Voronoi tessellation procedure to a single light optical section (compare Fig. 2 *a*, *cross*) of a typical human amniotic fluid cell nucleus (experiment 1, nucleus No. 9) with two painted and well-separated X territories. (a) Original image section. (*b*) Tessellation of the image into polygons is started with a few randomly distributed points, called the Voronoi generators (*white dots*). Each generator provides the center of a polygon. All image points contained in a given polygon are closer to the respective generator than to any other generator. The set of polygons established in this way represents the Voronoi diagram (compare *g*). (*c–e*) Examples of iterative Voronoi tessellation steps 2, 5, and 10 (final step). At each step, the variance of gray values in a given polygon is determined from all corresponding pixels. If the variation exceeds a preset value, the polygon is further subdivided. The division of the image into smaller and smaller polygons is continued until each polygon represents an area of image points (pixels) with similar gray values. (*f*) The image of the painted chromosome territories was extracted from the final Voronoi diagram by showing all polygons with a medium gray value above a defined threshold. (*g*) Schematic view of a Voronoi diagram (*solid lines*) and the corresponding Delaunay graph (*dashed lines*). The dots represent the localization of the generators for each Voronoi polygon. The generators of neighboring polygons (i.e., polygons that share a common edge) are connected in the Delaunay graph.

Figure 2. (*a*) Light optical serial sections (from top to bottom) through a female amniotic fluid cell nucleus with two painted X territories (experiment 1, nucleus No. 9). The Xi territory (*left*) was identified by its colocalization with the DAPI-stained Barr body (*arrows*). (*b–e*) Computer graphical 3D visualizations by raytracing of chromosome X territories from the nucleus shown in *a* after 3D Voronoi tessellation into polyhedras (see Materials and Methods) and segmentation at a median threshold. Territories are false colored in red (Xi) or yellow (Xa). The X territories are viewed in the x-y direction (*b*), y-z direction (*c*), and x-z direction (*d*). (*e*) An x-z direction view from the opposite side as shown in *d*. Bar: (*a*) 10 μm.

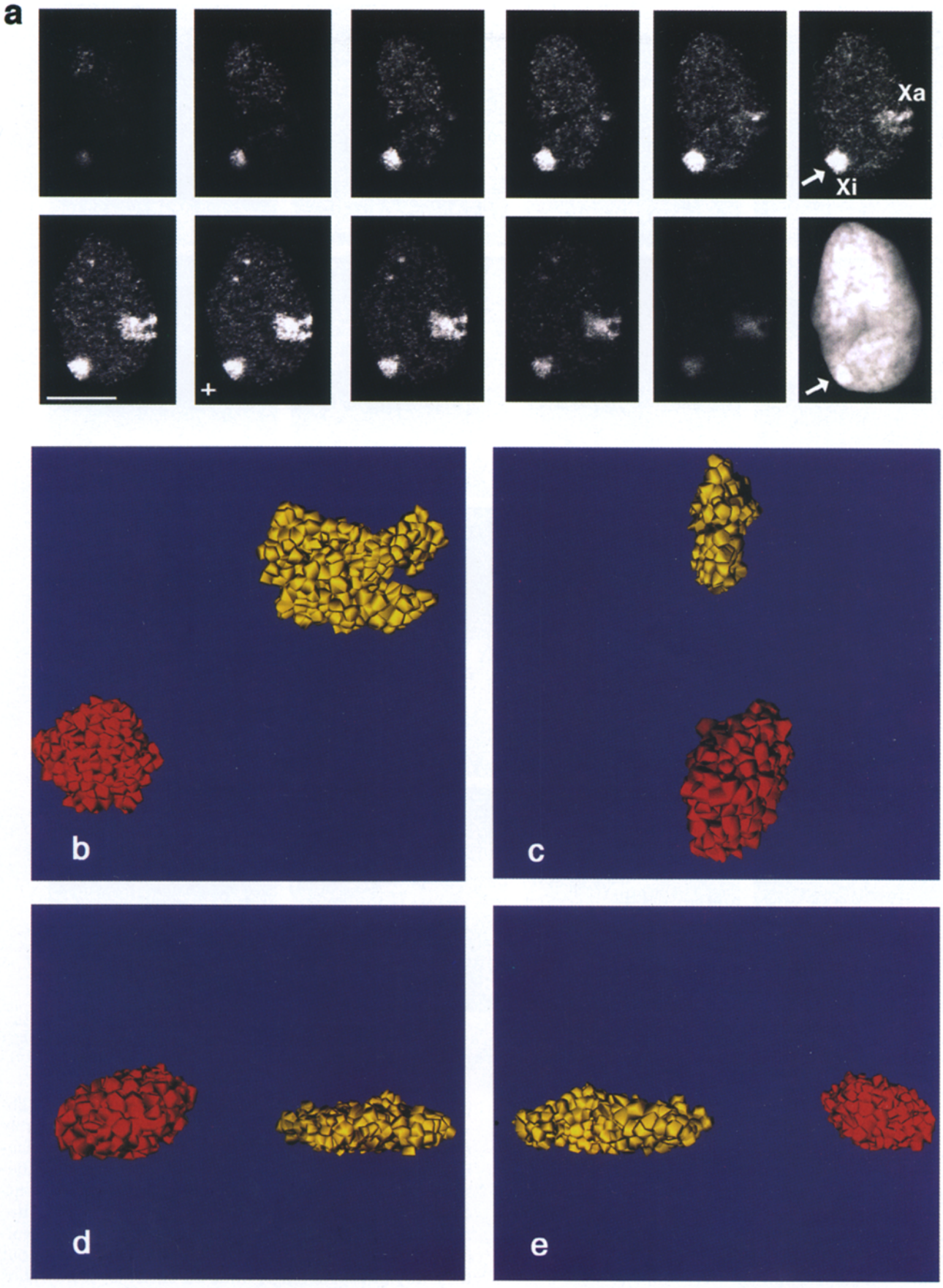
a
Xa
Xi
+
b
c
d
e

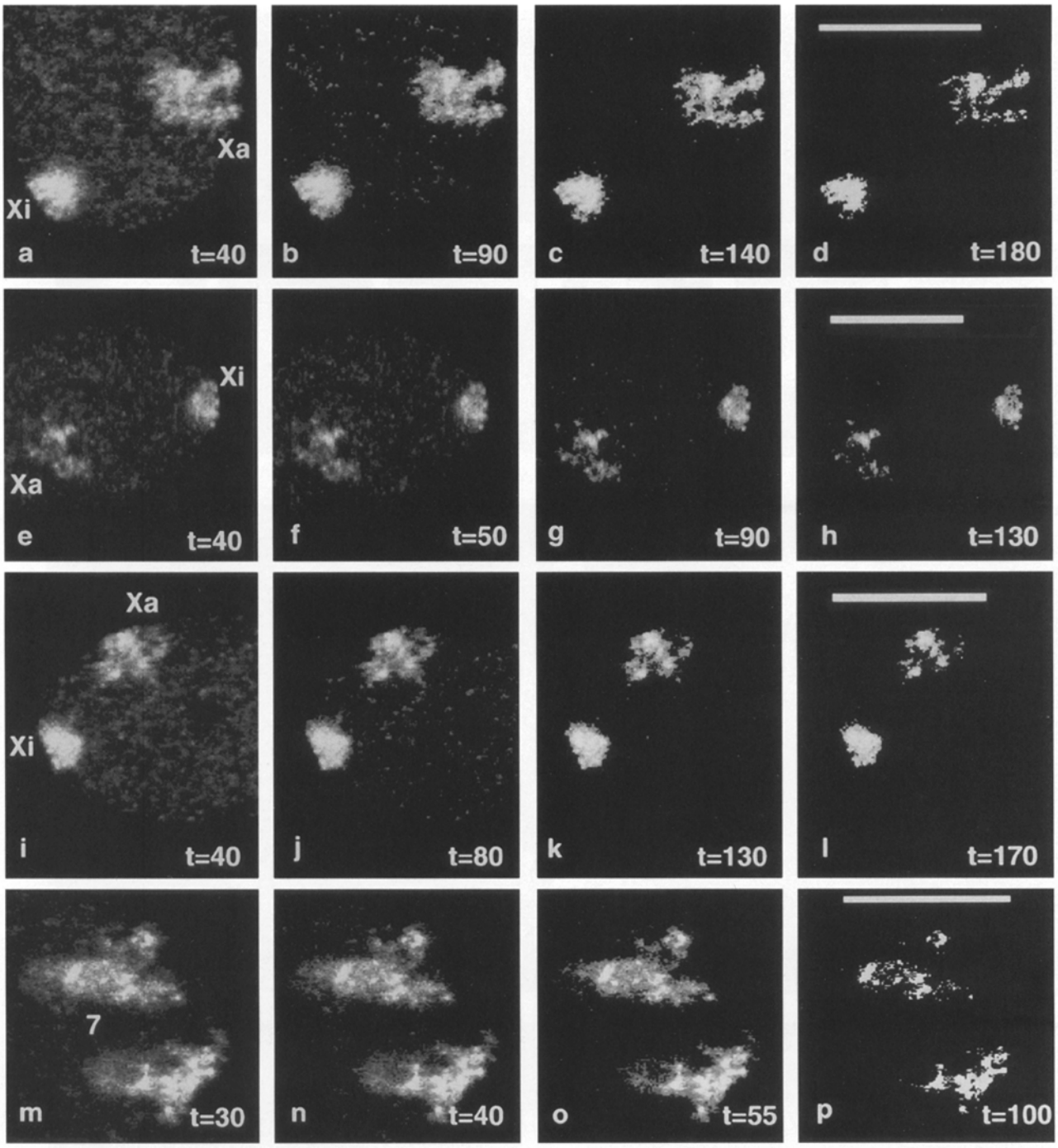

Figure 3. Light optical sections shown at different threshold levels. *a–d* (compare Fig. 2), *e–h*, and *i–l* show median sections through three nuclei with painted X territories. (*m–p*) Median section through a nucleus with painted chromosome 7 territories (compare Fig. 9 *a*).

ties are taken into account. The lower limit was defined by the threshold where at least one chromosome territory started to fuse with polyhedra apparently belonging to the background. Volumes recorded for lower thresholds would apparently result in an overestimation. Fig. 4 demonstrates the effect of the reasonable range of thresholds on volume, surface area, and roundness factor estimates of the painted X territories for the nucleus shown in Fig. 2. Absolute volume and surface area estimates were highly threshold dependent (Fig. 4, *a* and *b*). In contrast, *RF* values showed little variation over the entire threshold range (Fig. 4 *c*). The threshold-dependent variation noted for absolute volume and surface area estimates was considerably reduced when volume and surface area ratios were calculated for the two territories (Fig. 4 *d*). For each nucleus described below, chromosome territory volumes, surface areas, and roundness factors were averaged over the entire reasonable threshold range. Estimates for territory volumes and surface areas typically varied ± 30% throughout the entire threshold range, while the variation of the ratios of these morphological parameters for homologous territories was <10%, indicating that ratios are better suited

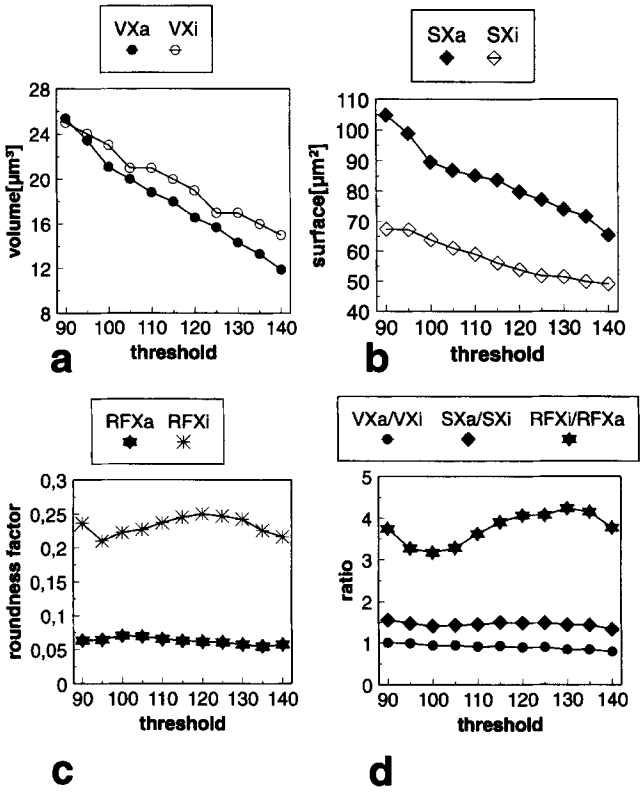

Figure 4. (*a–c*) For a range of reasonable thresholds (compare Fig. 3, *b* and *c*, and text), chromosome territory volumes, surface areas, and roundness factors were computed for the Xa and Xi territory of nucleus No. 9 (compare Fig. 2). *d* shows the respective ratios.

to judge volume and surface area differences between painted chromosome territories. Similar volume ratios were obtained for cells fixed with either 4% buffered formaldehyde or with methanol/acetic acid (3:1, vol/vol) (Rinke et al., 1995). This indicates that volume ratio measurements are relatively robust even against the shrinkage effects induced by the latter type of fixation.

Fig. 5 summarizes the volume, surface area, and roundness factors for the Xa and Xi territories studied in the 67 Barr body–positive nuclei (experiments 1, 2, and 3a). These experiments consistently indicated small volume differences between Xa and Xi territories (Fig. 5 *a*). Accordingly, volumes did not provide a useful parameter for the discrimination of Xa and Xi territories in these nuclei. A discrimination, however, could be based on differences in the territory surface areas (Fig. 5 *b*) and most reliably on differences in *RF* values (Fig. 5 *c*). The X territory that colocalized with the Barr body (Xi) provided the larger *RF* in 64 of 67 nuclei.

Similar Volumes and Differences in Shape and Surface Are also Noted for the Two X Territories in Barr Body–negative Cell Nuclei

The Barr body–positive nuclei studied in experiments 1, 2, and 3a comprised only a minor fraction (~30%) of the entire population of nuclei. To rule out a selection bias that favored the recognition of a Barr body in those nuclei where the Xi territory had a small lateral diameter but extended through the nucleus from top to bottom (Fig. 2 *a*), we wished to know whether nuclei chosen without reference to a recognizable Barr body would show a similar variability with regard to X territory volume, surface area, and roundness factor ratios. For this purpose, we studied these parameters in an additional sample of 55 nuclei exhibiting two separated, well-painted X territories without Barr body identification (experiment 3b). In each nucleus, the X territory with the larger *RF* was designated as Xr, discriminating the territory with the rounder shape from the territory with the more eccentric shape (Xe). A comparison of the respective ratios between samples of nuclei with and without Barr body identification showed a similar variation in both samples (Fig. 6, *a–c*).

Cumulative frequency curves for volumes, surface areas, and roundness factors obtained for Xe and Xr territories in experiment 3b are shown in Fig. 7, *a–c*. For comparison, Fig. 8, *a–c* shows the corresponding frequency curves for Xa and Xi territories in the 42 Barr body–positive nuclei studied in experiment 2. The Kolmogorov-Smirnov two sample test (Young, 1977) was applied to determine confidence levels for differences between Xe and Xr territories, as well as Xa and Xi territories. We requested $P < 0.01$ for a significant difference and $P < 0.001$ for a highly significant difference. In agreement with the cumulative frequency curves obtained for the volumes of Xa and Xi territories, the respective curves for Xe and Xr territories did not significantly differ ($P < 0.1$ and $P < 0.05$; compare Fig. 7 *a* with Fig. 8 *a*). The maximum distance between cumulative frequency curves plotted for the surface areas of Xe and Xr territories (Fig. 7 *b*) was similar to the highly significant maximum distance noted between the respective curves for the Xa and Xi territories (Fig. 8 *b*). A comparison of Fig. 7 *c* with Fig. 8 *c* shows that the maximum distance between the *RF* frequency curves for Xr and Xe territories was again similar to the highly significant maximum distance between the *RF* frequency curves for Xa and Xi territories. Fig. 7 *d* (*black columns*) shows the *RF* histogram of all 112 chromosome X territories studied in experiment 3b. Two clearly separated peaks can be seen. The first peak corresponds with the *RF* values of the Xa territories studied in experiment 3a (*white columns*), while the second peak corresponds with the Xi territories (*shaded columns*). The comparisons described in this paragraph support two conclusions. Firstly, Xe corresponds to Xa and Xr to Xi, and secondly, the 3D morphology differences between Xa and Xi territories are not limited to a subpopulation of nuclei with recognizable Barr bodies. They are a feature of the entire cell population (see Discussion). The prominent visibility of DAPI-stained Barr bodies in some but not all nuclei apparently does not depend on global differences in volume and shape, but on more subtle structural differences (see Discussion).

Comparison of Volume, Surface, and RF Estimates for Chromosome 7 and X Chromosome Territories

In experiment 2, we painted the chromosome 7 territories in addition to the X territories. To facilitate the comparison with data for Xa (= Xe) and Xi (= Xr), the chromosome 7 territory with the smaller *RF* was arbitrarily desig-

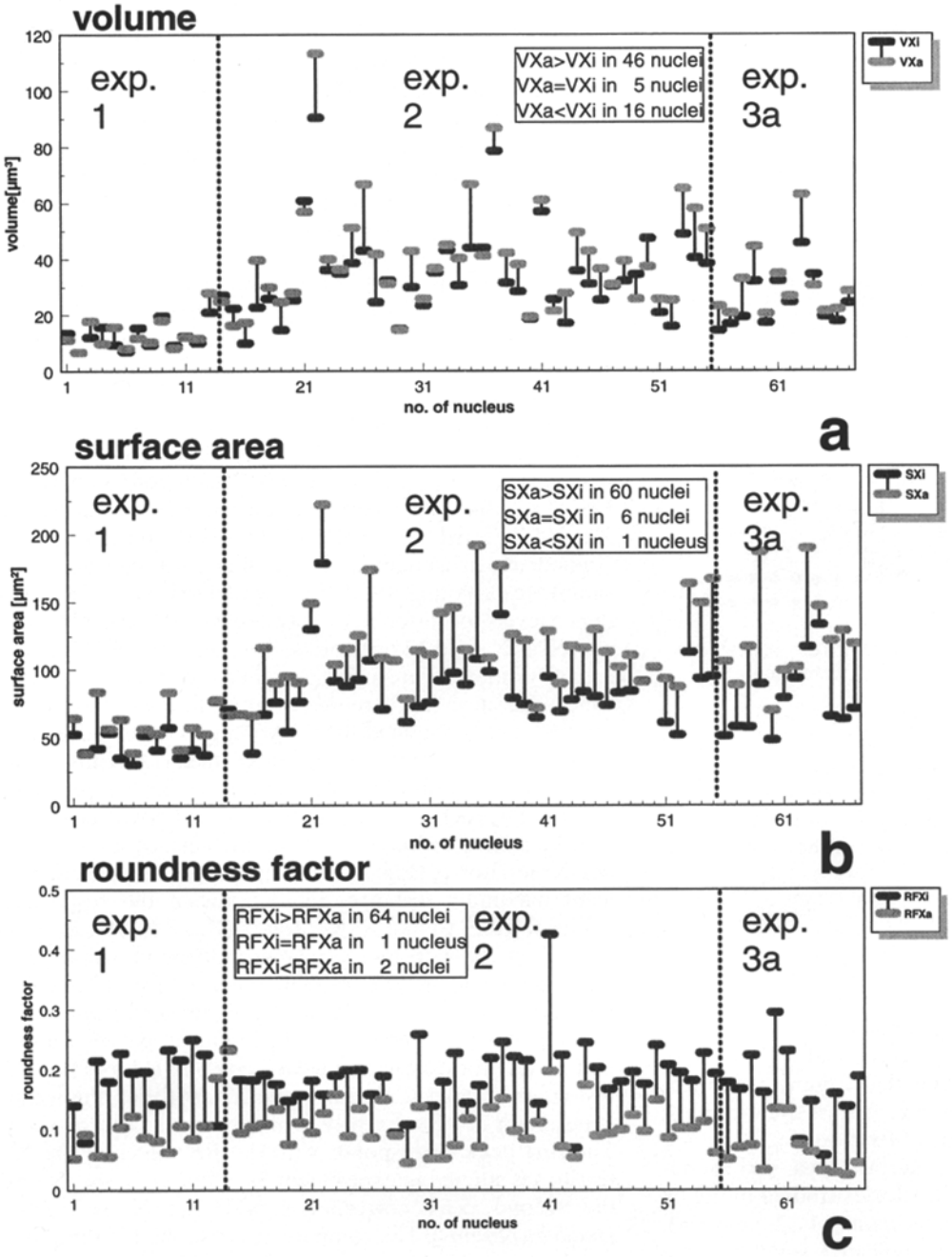

Figure 5. Morphological parameters calculated for 3D-reconstructed, painted Xa and Xi territories in 67 nuclei evaluated in experiment 1 (12 nuclei), experiment 2 (42 nuclei), and experiment 3a (13 nuclei). Abscissa: number of each nucleus. Ordinate: (*a*) volume, (*b*) surface area, and (*c*) roundness factor. The data indicate that Xa and Xi territories can be discriminated by surface and shape differences, but not by volume differences.

nated as 7e in each nucleus and discriminated from the territory with the larger *RF* (7r). Fig. 9 *a* shows a typical nucleus with simultaneously painted chromosome X and chromosome 7 territories. 3D reconstructions from different angles (Fig. 9, *b–e*) demonstrate that the 3D morphology of both chromosome 7 territories in this nucleus was similar to the 3D morphology of the Xa territory, but differed distinctly from the 3D morphology of the Xi territory. This finding was confirmed by the quantitative evaluation of the entire sample of 42 nuclei (Fig. 8, *a–c*). The volumes (Fig. 8 *a*) and surface areas (Fig. 8 *b*) recorded for the 7e and 7r territories were not detectably different from each other ($P > 0.1$), but significantly (7e; $P < 0.005$) or highly significantly (7r; $P < 0.001$) larger than the respective values obtained for the Xi territories. In contrast, significant volume differences between chromosome 7 territories and Xa territories were not found ($P < 0.05$ for Xa vs. 7r; $P < 0.1$ for Xa vs. 7e). With regard to surface areas, a highly significant difference was noted between chromosome 7 territories and Xi territories. The surface area difference between 7e and Xa territories was much less pronounced but still significant ($P < 0.01$). No significant surface area difference was obtained for 7r and Xa territories ($P > 0.1$). As expected, *RF* values (Fig. 8 *c*) recorded for the 7e and 7r territories showed a significant difference ($P < 0.005$). Notably, this difference was less pronounced than the highly significant difference between the *RF* values of Xa and Xi territories. *RF* values for 7r and 7e terri-

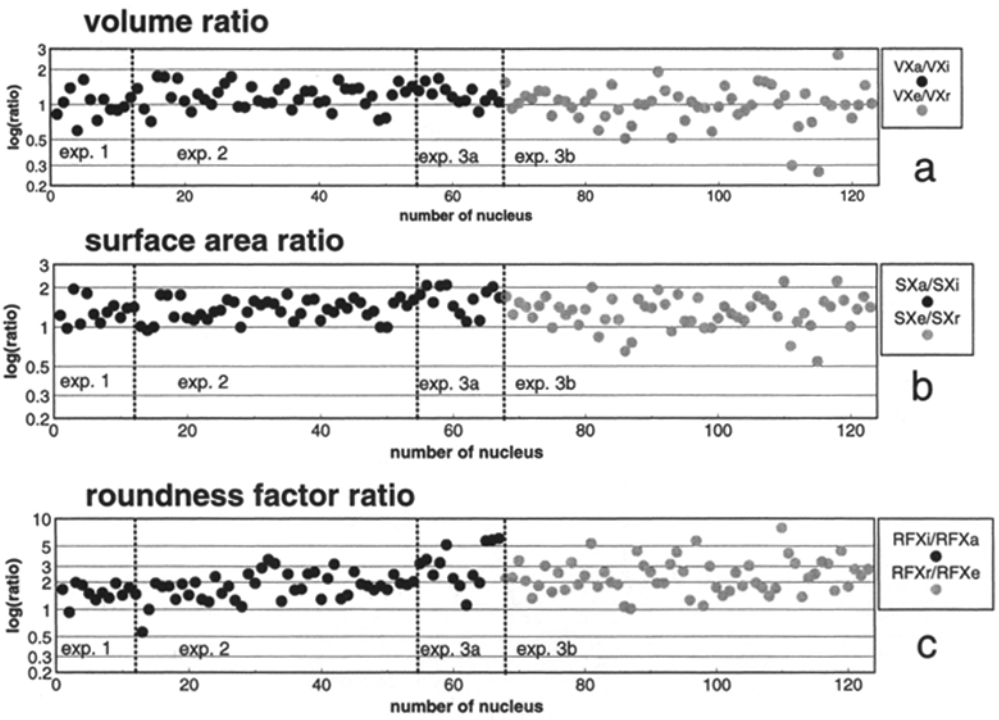

Figure 6. Ratios of morphological parameters (volume, surface area, and roundness factor) computed for the 3D-reconstructed X territories in 123 female amniotic fluid cell nuclei. Ratios are shown for 67 nuclei showing colocalization of a Barr body with the painted Xi territory (experiment 1, 2, and 3a; compare Fig. 5). X chromosome territories were also 3D reconstructed in a sample of 56 nuclei evaluated without Barr body discrimination (experiment 3b). For each nucleus, Xr designates the territory with the higher *RF*, Xe with the lower *RF*. Note that all RFXr/RFXe ratios are >1 by definition. Ordinate (logarithmic scale): (*a*) volume ratios, (*b*) surface area ratios, and (*c*) RF ratios. Abscissa: number of each nucleus.

tories were highly significantly different from the *RF* values for Xi territories. In contrast, comparison with Xa territories yielded no significant differences ($P > 0.1$ for 7e vs. Xa and $P < 0.05$ for 7r vs. Xa).

Table I summarizes the mean values of volume, surface area, and roundness factor ratios for experiments 1–3. The mean *RF* ratio Xi/Xa for the 67 nuclei in which the Xi territory could be unequivocally defined by its colocalization with the Barr body was 2.2. For the chromosome 7 territories, the mean *RF* ratio 7r/7e was 1.4. The means of the surface area ratios SXa/SXi and S7e/S7r were 1.4 and 1.0, respectively. In contrast, the means of the volume ratios were similar for both chromosome pairs (1.2 and 1.1).

Discussion

Validity of the Experimental Approach to Estimate Volume, Shape, and Surface Area Differences between Chromosome Territories

Chromosome painting, laser confocal microscopy, and 3D Voronoi tessellation were applied to study the 3D morphology of active and inactive human X chromosome territories. The conditions used in our experiments were carefully adapted to maintain nuclear height and shape, the location and shape of nucleoli, as well as the positioning of centromeres in amniotic fluid cell nuclei (Cremer et al., 1993, Eils et al., 1995*a*; our unpublished data). These conditions likely require modification for use in other cell types. Our results demonstrate that the shape (*RF*) and surface area, but not the volume of the Xa and Xi territories differed significantly in amniotic fluid cell nuclei. In all aspects studied so far, the 3D morphology of Xa territories was more similar to chromosome 7 territories than to Xi territories. This conclusion was confirmed when volume, surface area, and shape parameters of chromosome X and chromosome 7 territories were measured using the classical Cavalieri approach (Rinke et al., 1995) instead of the Voronoi tessellation (Edelmann, P., and C. Cremer, unpublished data).

Several factors may have influenced surface area estimates of chromosome territories. A major concern was the efficiency of chromosome painting procedures to delineate entire chromosome territories and not just a territory core. The true territory surface area could be underestimated if certain chromatin protrusions or infoldings were not visualized. In case that numerous unpainted giant chromatin loops largely protruded from such a painted core, we expected that signals from subregional probes should often scatter around the segmented territory core. This expectation was not substantiated in studies performed with 3D-intact human cell nuclei implying cosmid probes for the dystrophin gene (Cremer et al., 1993; Kurz et al., 1996), for the ANT3 and ANT2 genes located at the pseudoautosomal region and Xq24-q25, respectively (Schiebel et al., 1994), as well as Xp and Xq telomere near YAC-probes (Dietzel, S., G. Little, and K. Sützler, manuscript in preparation). We noted that for medium thresholds considered optimal for territory segmentation, the fraction of signals observed remote from the territory surface was generally <5%. Signals recorded for some autosomal genes also colocalized in most cases (>95%) with the respective autosome territories (Eils et al., 1995*b*; Kurz et al., 1996). Even at the highest thresholds for which a reasonable segmentation of entire territories could be obtained, the fraction of noncolocalizing signals remained small (<10%) (see below). While these findings seem to indicate that entire chromosome territories were faithfully delineated in the present experiments, the question of whether chromatin loops from neighboring chromosome territories can intermingle to a different extent in various cell types and during various functional states remains un-

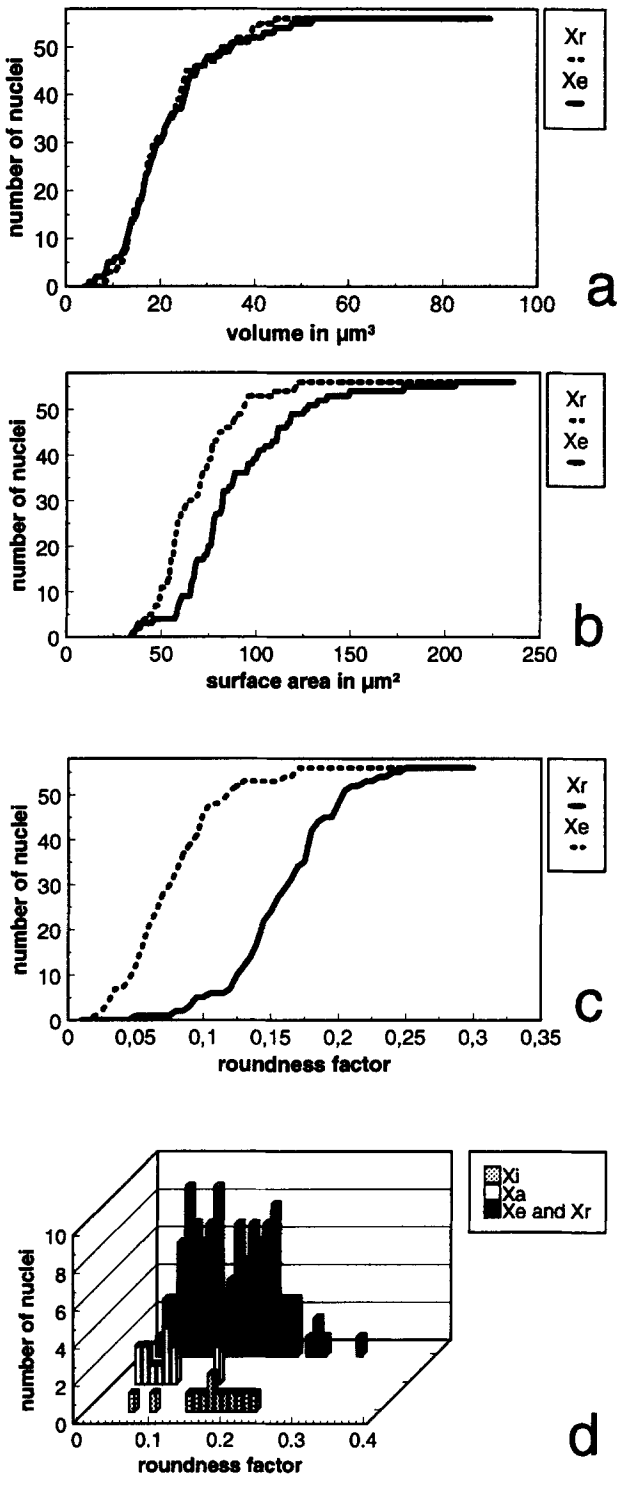

Figure 7. Cumulative graphs of the absolute values computed for the morphological parameters of the 112-chromosome X territories analyzed in experiment 3b. For definition of Xe and Xr, see legend to Fig. 6 and text. Abscissa: values obtained for a given parameter. Ordinate: number of nuclei. (*a*) Cumulative graphs for volume estimates of Xr and Xe territories. (*b*) Cumulative graphs for surface area estimates. (*c*) Cumulative graph for roundness factor estimates. (*d*) Histogram of the *RF* values for all X territories (*black columns*). Note two clearly separated peaks. In addition, the frequency distribution of *RF* values for all X territories evaluated in 13 nuclei of experiment 3a are shown. The distribution of RF_{Xi} (*shaded columns*) is clearly shifted towards larger values as compared to the distribution of RF_{Xa} (*white columns*).

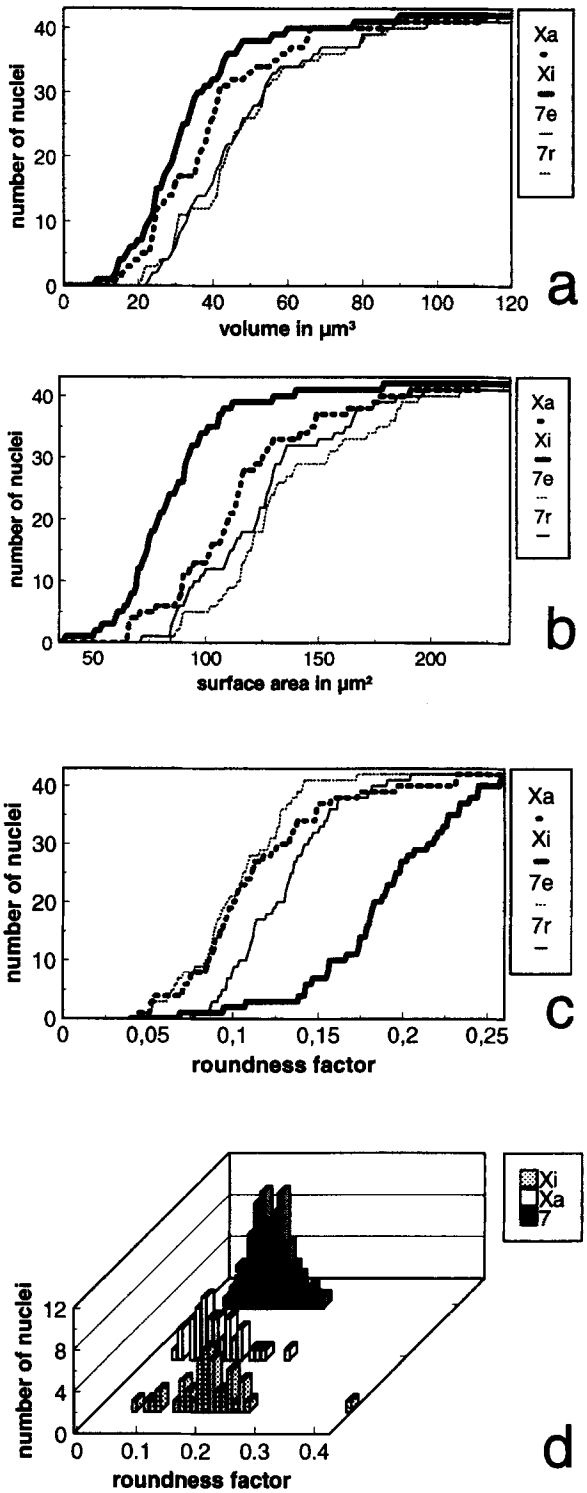

Figure 8. Volume, surface area, and *RF* parameters of the 84 chromosome 7 and X territories, respectively, analyzed in experiment 2. See text for definition of 7r and 7e. Abscissa: values obtained for a given parameter. Ordinate: number of nuclei. (*a*) Cumulative graphs for volume estimates. (*b*) Cumulative graphs for surface area estimates. (*c*) Cumulative graphs for roundness factor estimates. (*d*) Histograms of the *RF* values for chromosome 7 territories (*black columns*), Xa territories (*white columns*), and Xi territories (*shaded columns*).

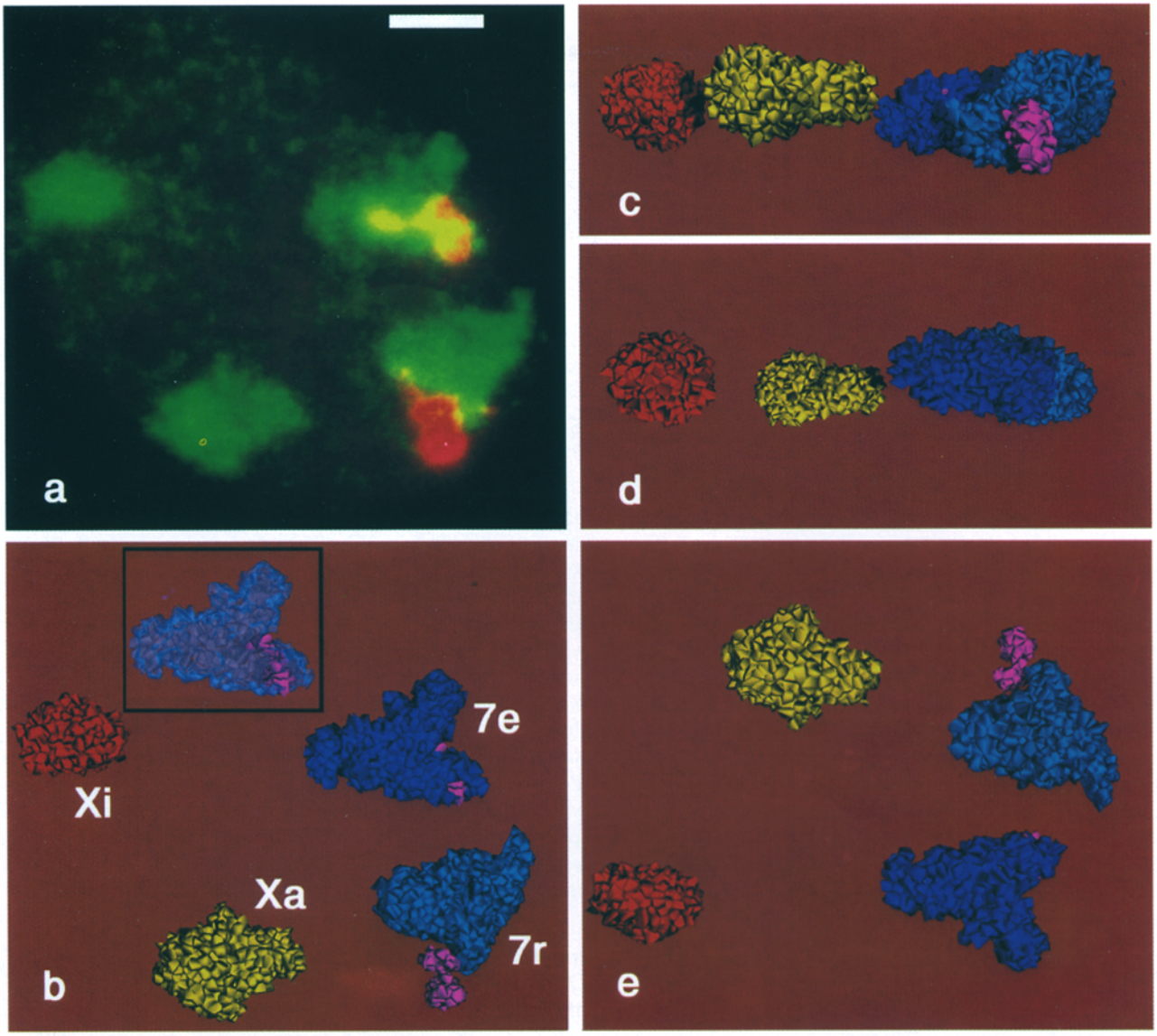

Figure 9. (*a*) Through-view composed of light optical serial sections of a a typical nucleus with green-painted chromosome 7 and X territories (experiment 2, No. 30). The chromosome 7–specific alphoid signal (*red*) unequivocally discriminates between the two chromosome 7 territories and the two X territories. (*b–e*) Computer graphical 3D visualizations by raytracing of segmented chromosome territories. (*b*) x-y direction, (*c*) x-z direction, (*d*) x-z direction from opposite side as shown in *c*, and (*e*) x-y direction view from opposite side as shown in *b*. False colors represent: red (Xi territory), yellow (Xa territory), light blue (7r territory) and dark blue (7e territory), and magenta (centromeric heterochromatin of chromosome 7). For definition of 7r and 7e, see text. Xa and Xi were discriminated by Barr body staining (not shown for this nucleus; compare Fig. 2 *a*). The black-bounded box in *b* shows a transparent view of the 7e territory, demonstrating part of the centromeric heterochromatin domain in the territory interior. Bar: (*a*) 5 μm.

solved and defines a focus for future studies of the functional nuclear architecture. For example, such studies will help to better understand the geometrical constraints involved in chromosomal rearrangements (Cremer et al., 1996).

The limited and different axial and lateral resolution of the confocal laser scanning microscope (~250 and 600 nm) also impairs the accuracy with which measurements of the 3D morphology of chromosome territories can be performed. Weighing the different sources of errors, which cannot be avoided with present technology, we assume that we likely underestimated the extent of shape and surface area differences that exist between the Xa and Xi territories (for further discussion see Bischoff et al., 1993; Eils et al., 1995*a*; Rinke et al., 1995).

3D Morphology Differences between Xa and Xi Territories Have a Complex and Still Unknown Molecular Basis

Similar volumes for Xa and Xi territories are compatible with the notion that higher order chromatin structures at a much smaller scale, e.g., a 50–100-kb loops, attain a decondensed chromatin configuration to allow the transcription

Table I. Mean Ratios of Volume, Surface, and Roundness Factors for X_a and X_i Chromosome Territories

	V_{Xa}/V_{Xi}	S_{Xa}/S_{Xi}	RF_{Xi}/RF_{Xa}	V_{7e}/V_{7r}	S_{7e}/S_{7r}	RF_{7r}/RF_{7e}
Mean ratio experiment 1 (12 nuclei)	1.03 ± 0.27	1.34 ± 0.28	2.48 ± 0.87			
Mean ratio experiment 2 (42 nuclei)	1.21 ± 0.28	1.37 ± 0.25	1.89 ± 0.63	1.09 ± 0.31	0.96 ± 0.21	1.40 ± 0.44
Mean ratio experiment 3a (13 nuclei)	1.23 ± 0.22	1.66 ± 0.34	3.43 ± 1.63			
	V_{Xe}/V_{Xr}	S_{Xe}/S_{Xr}	RF_{Xr}/RF_{Xe}			
experiment 3b (56 nuclei)	1.10 ± 0.36	1.42 ± 0.36	2.76 ± 1.36			

Mean ratios of volume, surface, and roundness factors (± standard deviation) obtained for Xa and Xi chromosome territories in Barr body–positive nuclei (experiment 1, 2, and 3a), for chromosome 7 territories (experiment 2), and for Xe and Xr territories in nuclei without Barr body assignment (experiment 3b).

of a gene residing in such a loop. Since even in Xa territories, only a small fraction of DNA represents actively transcribed genes, we can assume that not only in the Xi territory but also in the Xa territory, the large majority of the chromatin should be present in a configuration typical for inactive chromatin.

The stage of the cell cycle was not known for the nuclei chosen for 3D-reconstruction, raising the question whether the extent of differences between shape and surface area of Xa and Xi territories might change during the cell cycle. Additional studies using pulse labeling with iodide- and chlorine-labeled nucleotides together with chromosome painting in human diploid fibroblasts indicated that the 3D morphology difference between Xa and Xi territories described in the present study could also be noted during S-phase, even at a time when the Xi territory was still heavily replicating, while the Xa territory showed a weak incorporation of labeled nucleotides (Visser, A., and J.A. Aten, manuscript in preparation).

Walker et al. (1991) have noted a close association of the Xp and Xq telomeres in the Xi territory. This association should enforce a bent structure of the Xi territory, while its absence would allow the more extended structure of the Xa territory. The 3D morphology differences observed in the present study are consistent with this model. Recently, we performed distance and angle measurements for X specific centromeres and subtelomeric regions (Dietzel, S., G. Little, and K. Sätzler, manuscript in preparation). For both X territories, we noted a considerable variability of 3D distances between the centromere and subtelomere signals and the respective angles. These findings indicate that the 3D morphology differences noted for Xa and Xi territories have a more complex and still unknown molecular basis. Still unidentified protein–DNA, protein–RNA, and protein–protein interactions may play a role in the 3D organization of Xa and Xi chromosome territories.

Clemson et al. (1996) have noted that the Xi territory in human diploid fibroblast nuclei appears smaller than its active counterpart; however, this claim was not substantiated by 3D measurements. These authors have made two alternative proposals for the hypothetical large scale organization of the Xi territory: (*a*) The Barr body encompasses the entire Xi territory and regions of active (decondensed) chromatin are interspersed within the bulk of the Xi facultative heterochromatin. (*b*) Genes escaping X inactivation are organized in decondensed chromatin at the territory periphery, while the Barr body should colocalize with the compacted heterochromatic territory core. In the present study, inspection of light optical sections of painted Xa and Xi territories at different threshold levels indicated that some less intensely painted (less compacted?) DNA was located at the periphery of Xi territories surrounding a more compacted territory core. In Xa territories, domains with more and less intensely painted chromatin appeared to be distributed over the entire territory section. Further studies are required to test whether actively transcribed genes colocalize with the less intensely painted chromatin regions.

Implications of the 3D Morphology Differences between Xa and Xi Territories for Models of Chromosome Territory Organization

Models of interphase chromosome organization and nuclear architecture profoundly differ in their assumptions on the extent and functional implications of a large scale chromatin order (Manuelidis, 1990; Cremer et al., 1993, 1995; Zachar et al., 1993; Sachs et al., 1995). The 3D morphology differences between Xa and Xi territories were not predicted by the giant loop/random walk model (Sachs et al., 1995; Yokota et al., 1995). The larger and more complexly shaped surface of Xa territories lends some support to the view that chromosome territory surfaces play a functional role (Cremer et al., 1993, 1995; Zirbel et al., 1993; Kurz et al., 1996). Substantial tests of such a view require much more information on the compartmentalization of chromosome territories into distinct chromosomal subdomains, e.g., R- and G-band domains, and the 3D distribution of active and inactive genes. Further studies should also reveal whether more pronounced volume, shape, and surface area differences between the Xa and the Xi territory can be noted in other cell types, e.g., neurons, where many more X-specific genes are likely expressed than in amniotic fluid cells. It is also of interest in this context to study whether chromosome territories with similar DNA content but strongly different gene densities,

as is apparently the case for human chromosome 18 and 19 (Craig and Bickmore, 1994), show corresponding differences in their 3D structure.

Does XIST-RNA Provide a Clue for the 3D Organization of Xi Territories?

Differences in DNA methylation and histone acetylation, as well as differences in the timing of replication, have been implied in the maintenance of X inactivation in somatic cells as a clonally inherited feature (Gartler and Riggs, 1983; Grant and Chapman, 1988; Jeppesen and Turner, 1993; Disteche, 1995). The initiation of X inactivation is related to the presence of a unique region on the long arm of the human X chromosome (Xq13) known as the X inactivation center (for review see Heard and Avner, 1994). The *XIST* gene is located within the X inactivation center (Brown et al., 1991; for review see Rastan, 1994) and has been shown to be responsible for the initiation (Penny et al., 1996). *XIST* is actively transcribed on Xi but not on Xa and it is known that a functional RNA but no protein is formed. Most interestingly, the 3D distribution of XIST RNA is coincident with the 3D space occupied by the Xi territory, suggesting that XIST RNA has a structural role in the 3D organization of the Xi territory (Clemson et al., 1996). After removal of bulk chromatin, the XIST RNA was found closely associated with the insoluble nuclear matrix fraction indicating that it is not necessarily an integral component of the chromatin (Clemson et al., 1996). According to the interchromosomal domain compartment model (Cremer et al., 1995; see also Zachar et al., 1993), XIST RNA could be a component of interchromosonal domain channels. There is an urgent need to study the possible role of XIST RNA in Xi territory organization in more detail, including the stage when X inactivation occurs during early embryogenesis.

We thank Dr. J.-M. Chassery (University of Grenoble, Grenoble, France) for his continuous support in applying Voronoi diagrams as image analysis tools for painted chromosome territories and the Numerical Geometry group at the IWR, University of Heidelberg, in particular Dr. N. Quien, for support in computer graphics. The excellent technical assistance of M.-C. Meffert, H. Holtgreve-Grez, and G. Little is gratefully acknowledged.

This work was supported by the Deutsche Forschungsgemeinschaft (Cr 59/14-3; Cr 60/11-1) and the European Community (GENO-CT 91-0029 [SSMA] and BMH4-CT95-1139). R. Eils is the recipient of a postdoctoral fellowship from the Deutsche Forschungsgemeinschaft.

Received for publication 24 April 1996 and in revised form 10 September 1996.

References

Barr, M.L., and E.G., Bertram. 1949. A morphological distinction between neurons of the male and female, and the behavior of the nucleolar satellite during accelerated nucleoprotein synthesis. *Nature (Lond.).* 163:676–677.

Bischoff, A., J. Albers, I. Kharboush, E.H.K. Stelzer, T. Cremer, and C. Cremer. 1993. Differences of size and shape of active and inactive X-chromosome domains in human amniotic fluid cell nuclei. *Micr. Res. Tech.* 25:68–77.

Brown, S. W. 1966. Heterochromatin. *Science (Wash. DC).* 151:417–425.

Brown, C.J., A. Ballabio, J.L. Rupert, R.G. Lafreniere, M. Grompe, R. Tonlorenzi, and H.F. Willard. 1991. A gene from the region of the human X-inactivation centre is expressed exclusively from the inactive X chromosome. *Nature (Lond.).* 349:38–44.

Clemson, C.M., J.A. McNeil, H.F. Willard, and J.B. Lawrence. 1996. XIST RNA paints the inactive X chromosome at interphase: evidence for a novel RNA involved in nuclear/chromosome structure. *J. Cell Biol.* 132:259–275.

Collins, C., W.L. Kuo, R. Segraves, D. Pinkel, J. Fuscoe, and J.W. Gray. 1991. Construction and characterization of plasmid libraries enriched in sequences from single human chromosomes. *Genomics.* 11:997–1006.

Cooper, K.W. 1959. Cytogenetic analysis of major heterochromatic elements (especially Xh and Y) in *Drosophila melanogaster*, and the theory of "heterochromatin." *Chromosoma (Berl.).* 10:535–588.

Craig, J.M., and W.A. Bickmore. 1994. The distribution of CpG islands in mammalian chromosomes. *Nat. Genet.* 7:376–382.

Cremer, T., P. Lichter, J. Borden, D.C. Ward, and L. Manuelidis. 1988. Detection of chromosome aberrations in metaphase and interphase tumor cells by in situ hybridization using chromosome-specific library probes. *Hum. Genet.* 80:235–246.

Cremer, T., A. Kurz, R. Zirbel, S. Dietzel, B. Rinke, E. Schröck, M.R. Speicher, U. Mathieu, A. Jauch, P. Emmerich, et al. 1993. The role of chromosome territories in the functional compartmentalisation of the cell nucleus. *Cold Spring Harbor Symp. Quant. Biol.* 58:777–792.

Cremer, T., S. Dietzel, R. Eils, P. Lichter, and C. Cremer. 1995. Chromosome territories, nuclear matrix filaments and interchromatin channels: a topological view on nuclear architecture and function. *In* Kew Chromosome Conference IV. P.E. Brandham and M.D. Bennett, editors. The Royal Botanic Gardens, Kew, Richmond, Surrey, UK. 63–81.

Cremer, C., C. Münkel, M. Granzow, A. Jauch, S. Dietzel, R. Eils, X.-Y. Guan, P.S. Meltzer, J.M. Trent, J. Langowski, and T. Cremer. 1996. Nuclear architecture and the induction of chromosomal aberrations. *Mutat. Res.* In press.

Dietzel, S., E. Weilandt, R. Eils, C. Münkel, C. Cremer, and T. Cremer. 1995. Three-dimensional distribution of centromeric or paracentromeric heterochromatin of chromosomes 1, 7, 15, and 17 in human lymphocyte nuclei studied with light microscopic axial tomography. *Bioimaging.* 3:121–133.

Disteche, C.M. 1995. Escape from X inactivation in human and mouse. *Trends Genet.* 11:17–22.

Dyer, K.A., T.K. Canfield, and S.M. Gartler, 1989. Molecular cytological differentiation of active from inactive X domains in interphase: implications for X chromosome inactivation. *Cytogenet. Cell. Genet.* 50:116–120.

Eils, R., E. Bertin, K. Saracoglu, B. Rinke, E. Schröck, F. Parazza, Y. Usson, M. Robert-Nicoud, E.H.K. Stelzer, J.-M. Chassery, et al. 1995*a*. Application of laser confocal microscopy and 3D-Voronoi diagrams for volume and surface estimates of interphase chromosomes. *J. Microsc. (Oxf.).* 177:150–161.

Eils, R., K. Saracoglu, C. Münkel, J. Imhoff, K. Sätzler, E. Bertin, S. Dietzel, E. Schröck, T. Ried, T. Cremer, and C. Cremer. 1995*b*. Three-dimensional imaging approaches and Monte Carlo simulations: development of tools to study the morphology and distribution of chromosome territories and subchromosomal targets in human cell nuclei. *Zool. Stud.* 34(Suppl. 1):7–10.

Ferguson, M., and D.C. Ward. 1992. Cell cycle dependent chromosomal movement in premitotic human T-lymphocyte nuclei. *Chromosoma (Berl.).* 101: 557–565.

Gartler, S.M., and A.D. Riggs. 1983. Mammalian X-chromosome inactivation. *Annu. Rev. Genet.* 17:155–190.

Grant, S.G., and V.M. Chapman, 1988. Mechanisms of X-chromosome regulation. *Annu. Rev. Genet.* 22:199–233.

Heard, E., and P. Avner. 1994. Role play in X-inactivation. *Hum. Mol. Genet.* 3: 1481–1485.

Hulspas, R., A.B. Houtsmuller, P.J. Krijtenburg, J.G. Bauman, and N. Nanninga. 1994. The nuclear position of pericentromeric DNA of chromosome 11 appears to be random in G0 and nonrandom in G1 human lymphocytes. *Chromosoma (Berl.).* 103:286–292.

Ikizyan, I.A., S. Burde, and J.F. Leary. 1994. Interactive 3-D image analysis and visualization techniques for FISH-labeled chromosomes in interphase nuclei. *Bioimaging* 2:41–56.

Jauch, A., C. Daumer, P. Lichter, J. Murken, T. Schroeder-Kurth, and T. Cremer. 1990. Chromosomal in situ suppression hybridization of human gonosomes and autosomes and its use in clinical cytogenetics. *Hum. Genet.* 85: 145–150.

Jeppesen, P., and B.N. Turner. 1993. The inactive X chromosome in female mammals is distinguished by a lack of histone H4 acetylation, a cytogenetic marker for gene expresion. *Cell.* 74:281–289.

Kurz, A., S. Lampel, J.E. Nickolencko, J. Bradl, A. Benner, R.M. Zirbel, and P. Lichter. 1996. Active and inactive genes localize in the periphery of chromosome territories. *J. Cell Biol.* In press.

Lichter, P., and T. Cremer. 1992. Chromosome analysis by nonisotopic in situ hybridization. *In* Human Cytogenetics—A Practical Approach, 2nd ed., Vol. 1. D.E. Rooney and B.H. Czepulkowski, editors. IRL Press, Oxford. 157–192.

Lichter, P., T. Cremer, J. Borden, L. Manuelidis, and D.C. Ward. 1988. Delineation of individual human chromosomes in metaphase and interphase cells by in situ suppression hybridization using recombinant DNA-libraries. *Hum. Genet.* 80:224–234.

Lyon, M.F. 1961. Gene action in the X chromosome of the mouse (Mus muscukus L.). *Nature (Lond.).* 190:372–373.

Manuelidis, L. 1984. Different central nervous system cell types display distinct and nonrandom arrangements of satellite DNA sequences. *Proc. Natl. Acad. Sci. USA.* 81:3123–3127.

Manuelidis, L. 1990. A view of interphase chromosomes. *Science (Wash. DC).* 250:1533–1540.

Manuelidis, L., and J. Borden. 1988. Reproducible compartmentalization of individual chromosome domains in human CNS cells revealed by in situ hybridization and three-dimensional reconstruction. *Chromosoma (Berl.).* 96: 397–410.

Morton, N.E. 1991. Parameters of the human genome. *Proc. Natl. Acad. Sci. USA.* 88:7474–7476.

Muller, H.J., and S.M. Gershenson. 1935. Inert regions of chromosomes as the temporary products of individual genes. *Proc. Natl. Acad. Sci. USA.* 2:69–75.

Okabe, B., B. Boots, and K. Suguhara. 1992. Spatial Tessellations—Concepts and Applications of Voronoi Diagrams. John Wiley & Sons, New York. 532 pp.

Penny, G.D., G.F. Kay, S.A. Sheardown, S. Rastan, and N. Brockdorff. 1996. Requirement for XIST in X chromosome inactivation. *Nature (Lond.).* 379: 131–137.

Pinkel, D., J. Landegent, C. Collins, J. Fuscoe, R. Segarves, J. Lucas, and J.W. Gray. 1988. Fluorescence in situ hybridization with human chromosome-specific libraries: detection of 21 trisomy and of chromosome 4. *Proc. Natl. Acad. Sci. USA.* 85:9138–9142.

Quien, N., and W. Müller, 1992. Gothic vaults and transputers. *IEEE Comput. Graph. Appl.* 12:12–13.

Rappold, G.A. 1993. The pseudoautosomal regions of the human sex chromosomes. *Hum. Genet.* 92:315–324.

Rastan, S. 1994. X Chromosome inactivation and the Xist gene. *Cur. Opin. Genet. Dev.* 4:292–297.

Rinke, B., A. Bischoff, M.C. Meffert, R. Scharschmidt, M. Hausmann, E.H.K. Stelzer, T. Cremer, and C. Cremer. 1995. Volume ratios of painted chromosome territories 5, 7 and X in female human cell nuclei studied with confocal laser microscopy and the Cavalieri estimator. *Bioimaging* 3:1–11.

Sachs R.K., G. van den Engh, B.J. Trask, H. Yokota, and J.E. Hearst. 1995. A random walk/giant loop model for interphase chromosomes. *Proc. Natl. Acad. Sci. USA.* 92:2710–2714.

Saitoh, Y., and U.K. Laemmli. 1994. Metaphase chromosome structure: bands arise from a differential folding path of the highly AT-rich scaffold. *Cell.* 76: 609–622.

Scherthan, H., and T. Cremer. 1994. Nonisotopic in situ hybridisation in paraffin-embedded tissue sections. *In* Methods in Molecular Genetics, Vol. 5. K.W. Adolph, editor. Academic Press, New York. 223–238.

Schiebel, K., A. Mertz, M. Winkelmann, R. Nagaraja, and G. Rappold. 1994. Localization of the adenine nucleotide translocase gene ANT2 to chromosome Xq24-q25 with tight linkage to DXS425. *Genomics.* 24:605–606.

Spector, D.L. 1993. Nuclear organization of pre-mRNA processing. *Curr. Opin. Cell Biol.* 5:442–447.

Walker, C.L., C.B. Cargile, K.M. Floy, M. Delannoy, and B.R. Migeon. 1991. The Barr body is a looped X chromosome formed by telomere association. *Proc. Natl. Acad. Sci. USA.* 88:6191–6195.

Waye, J.S., S.B. England, and H.F. Willard. 1987. Genomic organization of alpha satellite DNA on human chromosome 7: evidence for two distinct alphoid domains on a single chromosome. *Mol. Cell. Biol.* 7:349–356.

Xing, Y., C.V. Johnson, P.R. Dobner, and J.B. Lawrence. 1993. Higher level organization of individual gene transcription and RNA splicing. *Science (Wash. DC).* 259:1326–1330.

Yokota H., G. van den Engh, J.E. Hearst, R.K. Sachs, and B. Trask. 1995. Evidence for the organization of chromatin in megabase pair-sized loops arranged in the human G0/G1 interphase nucleus. *J. Cell Biol.* 130:1239–1249.

Young, E.T. 1977. Proof without prejudice: use of the Kolmogorov-Smirnov test for the analysis of histograms from flow systems and other sources. *J. Histochem. Cytochem.* 25:935–941.

Zachar, Z., J. Kramer, I.P. Mims, and P.M. Bingham. 1993. Evidence for channeled diffusion of pre-mRNAs during nuclear RNA transport in metazoans. *J. Cell Biol.* 121:729–742.

Zirbel, R.M., U.R. Mathieu, A. Kurz, T. Cremer, and P. Lichter. 1993. Evidence for a nuclear compartment of transcription and splicing located at chromosome domain boundaries. *Chromosome Res.* 1:93–106.